Influence of co-existing species on charge transfer in dye-sensitized nanocrystalline oxide semiconductors in aqueous suspension for H$_2$ evolution under visible light

Masato M. Maitani*, Conghong Zhan, Dai Mochizuki, Eiichi Suzuki, Yuji Wada*

Department of Applied Chemistry, Graduate School of Science and Engineering, Tokyo Institute of Technology, 2-12-1 Ookayama, Meguro, Tokyo 152-8552, Japan

ABSTRACT

The water splitting under visible irradiation is of significant importance for the ultimate purpose of producing fuel from abundant water and the sunlight for the sustainable future society. The proper construction of an antenna for the efficient photon collection in the visible region and the reaction site for water splitting on the semiconductor surface has been desired and studied in order to design the efficient total system which enables the separation of photo-excited hole and electron, leading to the final redox reactions of water on the surface. In this paper, the dye-sensitized nanocrystalline oxide semiconductors of TiO$_2$, SnO$_2$, and ZnO are examined as the aqueous colloidal suspension for an application to the photocatalytic H$_2$ evolution under visible light (>390 nm) as a half-cell of water splitting system. The efficiency of H$_2$ evolution is strongly influenced by the combination of oxide semiconductors, dye-sensitizers, and co-existing electron donor species in the suspension system. We herein perform the detailed analyses based on the photochemical and photo-electrochemical measurements to elucidate the combinational effects. The charge transfer properties are discussed in terms of the kinetics involving the electron injection and charge recombination, which reveals rather conjugated effects caused by the specific combination of the dye-sensitizers and co-existing electron donor species with oxide semiconductors than the simple mechanisms based on the thermodynamics involving the energy level of conduction band relative to LUMO of dye-sensitizers. The inversed results of H$_2$ evolution between TiO$_2$ and SnO$_2$ with two kinds of electron donor species (alcohol and amine) are also analyzed in detail in terms of the charge transfer processes of dye-sensitized nanocrystalline oxide semiconductors in the suspension systems.

© 2013 Elsevier B.V. All rights reserved.

1. Introduction

Artificial photosynthetic systems for direct conversion of water to obtain an energy source, hydrogen, under sunlight are of great interest and importance as a candidate among the technologies for creating renewable energy used in the future. Wide-band gap nano-sized semiconductor materials such as metal oxide, nitride, and sulfide derivatives have been widely studied to harvest light to generate electrons with high energy capable of reduction of protons to H$_2$ and holes consumed in oxidation of sacrificial electron donors, redox shuttles, or water [1–3]. The advantages of these oxide semiconductors are robustness, abundance of materials, ease of preparation, and non-toxicity. The absorption of band gap transition typically ranges in the ultra-violet region with these

semiconductors, while most photon flux from the sunlight ranges widely in visible and infrared regions. Therefore harvesting photons in visible and infrared region is one of the most important issues when these semiconductors are employed as a photocatalyst.

As summarized elsewhere [1–4], a few strategies have been proposed to achieve higher photon collection efficiency under sunlight, *i.e.* (1) introduction of inter-band states by doping, (2) adjustment of band structures by introducing hetero metallic oxide, and (3) dye-sensitization by chromophore molecules. Among these, the sensitization of the semiconductors by metal complex and organic dye molecules has elegantly enabled the high solar energy conversion efficiency of ∼13% owing to the almost 100% internal quantum efficiency in the photon-to-electron conversion process in the visible region, 400–700 nm, for a photovoltaic device known as the dye-sensitized solar cells [5,6]. In addition, recent reports revealed that the durability problem of dye-sensitizers is possibly overcome by using robust dye-sensitization system revealing continuous H$_2$ evolution for more than hundreds of hours [7,8]. Furthermore even the complete water splitting, both H$_2$ and O$_2$ evolution, has been

also achieved with dye-sensitization system by applying the transition metal oxide catalysts, such as iridium oxide as a reaction site for O_2 evolution [9–11]. Nevertheless, the efficiency of the dye-sensitization system is limited by the low rate of H_2 evolution, resulted from the poor electron transport process in the system preceded by the efficient light absorption. Further understanding of the electron transport process in dye-sensitization system is thus desired to increase the photon to hydrogen conversion, since the photon harvesting efficiency is already ensured to be 100% in the visible and near IR region of solar spectrum in this system [5,6]. The electron transport processes of dye-sensitization system for H_2 evolution following the photon absorption by dye-sensitizer are composed of (1) electron injection from dye to semiconductor, (2) electron diffusion in semiconductor (toward catalysts placed on the surface of semiconductors such as Pt), (3) proton reduction on the surface, and (4) regeneration of the dye through reduction by redox shuttles or sacrificial electron donors in addition to unfavorable reactions such as (5) dye deactivation and (6) recombination of separated electron and hole.

In addition to the effective photon collection efficiency, one advantage of the dye-sensitization system is considered as the ultrafast charge separation producing an electron and a hole at the dye–semiconductor interface [6]. Furthermore, the spatial charge separation achieved by the electron injection from dye-sensitizers into semiconductors dramatically suppresses the charge recombination of electrons and holes. The charge separation process is thus efficient enough to reach 100% quantum yield in the dye-sensitization system [4,6]. The electron injection occurs from the lowest unoccupied molecular orbital (LUMO) locating at more negative chemical potential than that of the conduction band (CB) of semiconductors [6,12]. Therefore, the injection efficiency is closely related to the potential gap between CB and LUMO [13–16]. It is however observed that the electron injection strongly affecting on the efficiency of the photoelectric conversion also depends on other factors, e.g. aggregation of dye molecules on the surface, the co-existing species and its adsorption on the surface of semiconductors, and solvent effects [17–21]. It is thus generally considered that the dye-sensitization system has not been completely understood especially in case co-existing species are involved in the system [22–25]. This led us to a previous study to comprehend the complex system including co-existing species, e.g. contaminants, acid, base, electrolytes, etc., in dye-sensitized photocatalytic water splitting process for the realistic applications [26,27]. We recently reported that the electron injection process of dye-sensitization system strongly depends on the co-existing species, methanol (MeOH) and triethanolamine (TEOA), as the sacrificial electron donors in surrounding solution for the photocatalytic H_2

evolution [28–30]. Additionally, it was found that the capability of H_2 evolution cannot be attributed to only electron injection efficiency but also other electron transfer processes at the dye/TiO_2 interface. We found the effects of metal oxide in dye-sensitization system on H_2 evolution, and revealed opposite results of H_2 evolution with dye-sensitized TiO_2 and SnO_2 either in TEOA or MeOH solution [28]. These results cannot be understood with the conventional model based on the thermodynamics, that is, differences in conduction band potential of TiO_2 and SnO_2, LUMO positions of dyes referred with conduction band of nanoparticle semiconductors, absorption wavelength of dye-sensitizers, etc., as the determinants of the down-hill forward process of electron transfer and the photon harvesting process, respectively.

We herein perform detailed photochemical, electrochemical, and photoelectrochemical analyses to understand the charge transfer characteristics in dye-sensitized metal oxide systems. According to the results, the co-existing electron donor species, MeOH and TEOA, in the surrounding medium strongly influence on the kinetics of the electron injection and charge recombination at the interface between the dye-sensitizers and oxide semiconductor nanoparticles and the adsorption–desorption nature of dye-sensitizers [29,30], in addition to the thermodynamic energetics of the band structures of semiconductor nanoparticles. It was thus found that the capability of H_2 evolution cannot be ascribed with the simple mechanism only with the potential but also the kinetics of competitive charge transfer processes strongly influenced by the surface chemical properties. We therefore discuss the combinational effects between the dye-sensitizers, semiconductor nanoparticles, and donor species in the surrounding medium on the electron transport processes in photocatalytic H_2 evolution as the half-cell of the water splitting system.
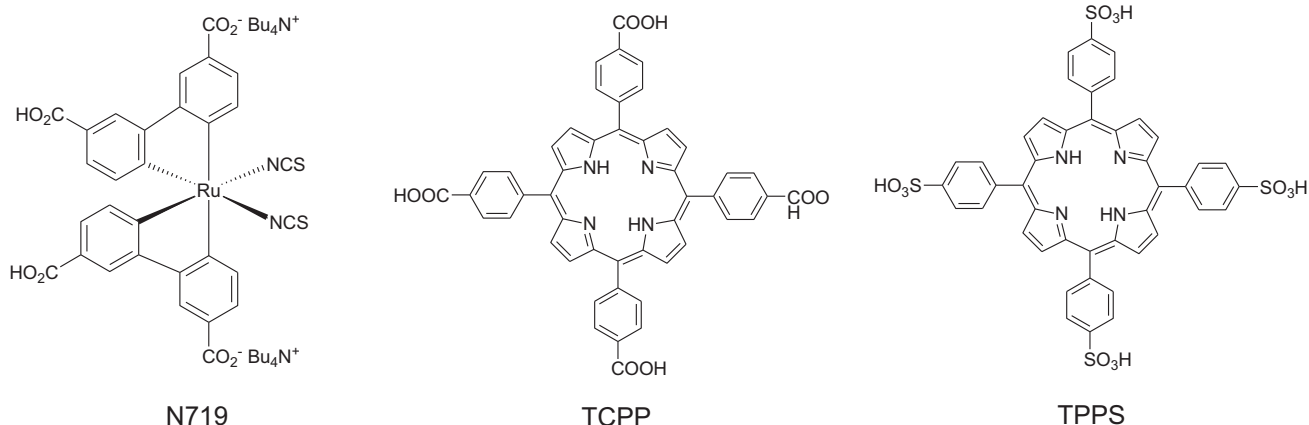
2. Experimental

2.1. Materials

The commercially available TiO_2 particles (P25, Nippon Aerosil), dye-sensitizers, $(n\text{-}Bu_4N)_2\text{-}cis\text{-}Ru(dcbpy)_2(SCN)_2$ (N719, Solaronix, Switzerland), tetrakis(4-carboxyphenyl)porphyrin and tetrakis(4-sulfonatophenyl)porphyrin (TCPP and TPPS, respectively, Tokyo Kasei) (Scheme 1) were used as purchased without any further purification.

2.2. Sample preparation

SnO_2 nanoparticles were synthesized by the microwave heating [31]. White tin hydroxide precipitate was obtained by adding

Scheme 1. Dye-sensitizers.

an aqueous ammonia solution (6 M) to adjust the pH value of the precursor solution composed of Tin(IV)chloride pentahydrate ($SnCl_4 \cdot 5H_2O$, 1.9 g) and polyvinylalcohol (PVA, 1 wt%) in deionized water (180 mL) to be about 9–10. After the precipitated hydroxide was heated at the MW power of 750 W for 10 s in a microwave apparatus (MicroSYNTH, Milestone General), the mixture became clear in appearance. This clear solution was irradiated by MW at the power of 750 W for 1 min to boil the solution and was kept at the boiling point by maintaining the microwave power for another 1 h, leading to the formation of the white precipitates. After cooling the sample mixture, the precipitate was washed by the decantation with deionized water until no chloride ion was detected in the filtrate (tested by 0.1 M $AgNO_3$ solution), and then the solvent was replaced with ethanol once. The final white powdery products were dried under the microwave irradiation with the power of 750 W for 5 min. Calcination of the products was carried out at 300 °C for 2 h in a tubular furnace (S1).

For hydrogen evolution, loading of Pt on oxide semiconductors was carried out by a conventional photochemical deposition to obtain 1 wt% Pt-loaded TiO_2, SnO_2, and ZnO nanoparticles as described elsewhere [28,29]. The dye-sensitized Pt-loaded oxide nanoparticles were obtained by dispersing Pt-loaded oxide nanoparticles into 0.1 mM of dye-sensitizers in methanolic solution, kept for 48 h under dark, filtrated, washed with deionized water, and then dried at 80 °C. The adsorption isotherm of the dye-sensitizers on TiO_2 revealed monolayer chemisorption through carboxylic and sulfonic acid moiety of the dyes (S2). For photoelectrochemical analysis, the films made of dye-sensitized porous oxide nanoparticles were prepared by the conventional doctor blade technique by using commercially available TiO_2 paste (Ti-nanoxide D, Solaronix) and home-made paste with SnO_2 nanoparticles on cleaned F:SnO_2 transparent conductive glass (TCO) and sintered at 450 °C for 30 min in atmosphere. When the temperature was dropped to 80 °C after sintering, these films were immersed into a 0.1 mM solution of dye-sensitizers in methanolic solution, kept under dark for 12 h, washed by ethanol, and then dried under N_2 flow.

SnO_2 colloidal paste was prepared by a typical procedure [32] as described below. The washed SnO_2 (dry weight: 1 g) was dispersed in deionized water (8 g) containing polyethyleneglycol (MW: 2000, 0.9 g), and ultrasonicated for at least 30 min to prepare the well-dispersed colloidal SnO_2 paste.

2.3. Photocatalytic H_2 evolution

The H_2 evolution was performed in an outer irradiative photoreactor under Xe lamp (LC8, HAMAMATSU) irradiation through a cut-off filter ($\lambda < 390$ nm cut, UV-39, TOSHIBA). The dye-sensitized Pt-loaded oxide nanoparticles were dispersed in an aqueous solution (1 g/L) containing sacrificial electron donors, MeOH and/or TEOA. Prior to the irradiation, an ultrasonication for 5 min and consecutively argon bubbling for 15 min were applied to the reaction mixture. The evolved H_2 was analyzed by taking the sample gas from the photoreactor with a gas-tight syringe and injecting into a gas chromatography (molecular sieve 5A column with Ar carrier gas, GC-8A, Simadzu). As a controlled experiment with D_2O solution, all evolved hydrogen was D_2 ensuring that the hydrogen source was the protons in the water not from other compounds, such as donor species or dye-sensitizers. Another controlled experiment without dye-sensitizer also ensured that the residual UV light was negligible for H_2 evolution.

2.4. Fluorescence quenching analysis

The fluorescence spectra of each dye-sensitizer, TCPP and TPPS in the aqueous sacrificial donor solutions with varying the

density of TiO_2 and SnO_2 colloids were measured to study the fluorescence quenching due to the electron injection processes from the photoexcited dye-sensitizers. The oxide semiconductor nanoparticles stock suspensions in water (~4 g/L) were prepared by ultrasonication for more than 30 min giving well-dispersed colloidal suspension. The fluorescence spectra of dye-sensitizer in aqueous solution were collected in a 1 cm-quartz-cell under photoexcitation ($\lambda_{ex} = 410$ nm (TCPP) and 415 nm (TPPS), F7000, Hitachi). The specific amount of the oxide stock suspension was successively added dropwisely into the dye-sensitizer solution and then the fluorescence spectra were measured after waiting for 15 min to reach equilibrium. The concentrations of either TEOA in MeOH (6.2 M) or MeOH in TEOA (0.3 M) were also varied to determine the effect of co-existing electron donor species on the fluorescence of dye-sensitizers. All spectral measurements were carried at room temperature out after 15 min Ar purge. The intensity of fluorescence was determined at the peak top locating at around ~650 nm.

2.5. Electrochemical analysis

The electrochemical and photoelectrochemical analysis were carried out with dye-sensitized films composed of TiO_2 nanoparticles as a working electrode in a three component electrochemical cell with the aqueous electron donor solution containing 0.1 M of KCl as supporting electrolyte. Pt counter electrode, and a reference electrode, Ag/AgCl, were used with an electrochemical potentiostat (SP-200, Bio-Logic) therein. Ar babbling was applied for 15 min prior to each measurement. A Xe lamp (MAX-302, Asahi bunko) with a cut filter (<410 nm cut, UV-41, TOSHIBA), was used as a visible light source. The residual UV light was confirmed to be negligible by a controlled experiment without dye-sensitizer on TiO_2 film.

3. Results and discussion

3.1. H_2 evolution

During the H_2 evolution carried out under a visible light source, the accumulated H_2 gas as the product in the reaction vessel was sampled and quantitatively plotted as a function of the reaction time up to 3 h under visible light irradiation (>390 nm: Xe lamp) based on the analysis with gas chromatography as shown in Fig. 1. We confirmed that evolved hydrogen was originated from the proton of water in the solution not from other hydrogen sources, such as degradation of organic species in the solution or dye-sensitizer it self, in each of experimental condition (S3). Certain combinations of oxide semiconductors, sensitizers, and electron donors in the solution revealed continuous H_2 evolution for up to 3 h. A slight decline of the slope of the H_2 evolution was observed probably due to either the degradation or desorption of the dye dye-sensitizers during the photocatalytic reaction. As Fig. 1a indicates, all three sensitizers, N719, TCPP, and TPPS, on TiO_2 revealed continuous H_2 evolution in TEOA solution up to 3 h under visible irradiation, while TCPP and TPPS, however, revealed no H_2 evolution in MeOH solution, while N719 resulted in comparable reaction even in MeOH solution as we have reported recently [28,29]. Contrary to TiO_2, SnO_2 nanoparticles revealed completely opposite results in H_2 evolution as shown in Fig. 1b. In addition, ZnO did not produce any H_2 in any of each system (plot is not shown) as all data including TiO_2 and SnO_2 are summarized with H_2 evolution after 3 h irradiation (Table 1). Additionally, Fig. 1b exhibits that TEOA addition into the TCPP/SnO_2/MeOH system significantly degrades H_2 evolution. Since the composition of TEOA and MeOH can dramatically change the pH of surrounding solution (S4), a controlled experiment of pH dependences of TCPP/TiO_2/MeOH and TCPP/SnO_2/MeOH on
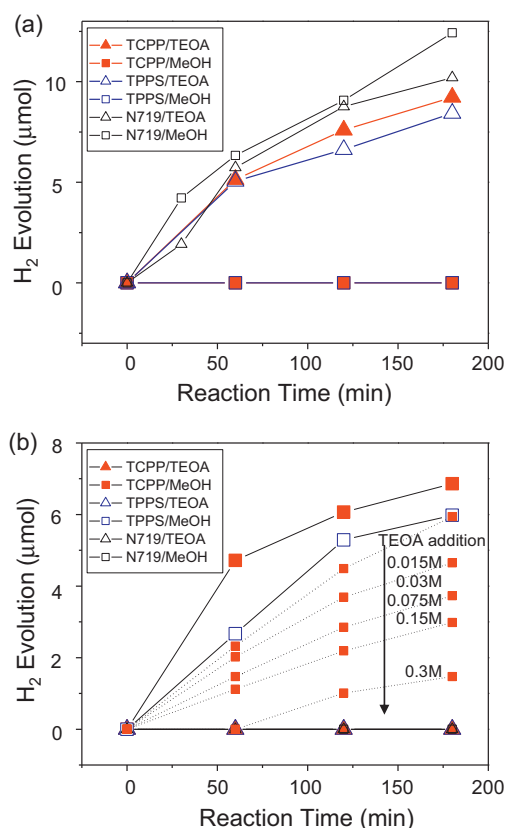
Fig. 1. H_2 evolution of dye-sensitizers, TCPP (filled red), TPPS (open blue), and N719 (open black) on (a) TiO_2 and (b) SnO_2 nanoparticles in donor solutions of MeOH (square) and TEOA (triangle) aqueous solution under visible light (>390 nm: Xe lamp). As an additional data, SnO_2/TCPP in MeOH with addition of either TEOA is also indicated with dashed lines. (For interpretation of the references to color in this figure legend, the reader is referred to the web version of this article.)

Table 1
H_2 evolution accumulated for 3 h in the reaction vessel under visible irradiation (>390 nm).

Oxide	Dye-sensitizer	Donor	H_2 evolution
	N719	MeOH	12.4
		TEOA	10.2
TiO_2/Pt	TCPP	MeOH	0
		TEOA	9.2
	TPPS	MeOH	0
		TEOA	8.4
	N719	MeOH	0
		TEOA	0
SnO_2/Pt	TCPP	MeOH	6.6
		TEOA	Trace
	TPPS	MeOH	5.1
		TEOA	Trace
	N719	MeOH	0
		TEOA	0
ZnO/Pt	TCPP	MeOH	0
		TEOA	0
	TPPS	MeOH	0
		TEOA	0

Light source: 150 W Xe lamp (>390 nm); irradiation time: 3 h; 1 g/L of oxide nanoparticles in 2.5 mL suspension with either MeOH (6.2 M) or TEOA (0.3 M) aqueous solutions.

H_2 evolution was performed (S5) and revealed that the results observed in our study is not directly related to the pH potentially affecting the conduction band level of oxide semiconductors as discussed in the later section. In addition, the porphyrin dye-sensitizer, TCPP and TPPS, posses the states of protonation and deprotonation with variation of pH in the surrounding medium. It was however revealed that the pH value within the experimental condition of TEOA and MeOH solution (S4) does not largely affect to the absorption characteristics of porphyrine-based dye-sensitizers (S6). Although both TEOA and MeOH are typical electron donors used in photocatalysts systems (E_{ox} = 0.2–0.7 V (MeOH) [33,34] and E_{ox} = 0.82 V (TEOA) [35] *vs.* NHE) and also HOMO levels of TCPP (0.96 V *vs.* NHE), TPPS (0.98 V *vs.* NHE), and N719 (0.85 V *vs.* NHE) are located closely [36–38], the resulted H_2 evolution shows clear difference depending on the combination of dye-sensitizers and co-existing electron donor species, TEOA and MeOH, in the colloidal nanocrystalline semiconductor aqueous suspensions (Table 1).

3.2. Fluorescence quenching analysis

To study the efficiencies of electron injection at dye-sensitizers/oxide semiconductor interface in each system, we employed a fluorescence quenching measurement of dye-sensitizers by addition of the electron acceptor, oxide nanoparticles, for the photo-excited electron transfer known as Stern–Volmer relation [15,39–42]. Because of the lack of fluorescence intensity with N719, we applied this analysis only to the systems with porphyrin/oxide nanoparticles colloidal suspension. Since each dye-sensitizer interacts with oxide nanoparticles with certain association constants, K_{app} [15,29,30], we apply the reciprocal Stern–Volmer relation under a consideration of an association constant, as indicated by Eq. (1), where I_{surf} represents the fluorescence intensity of dye-sensitizer in case all of dye molecules in the system is adsorbed on the quencher, oxide nanoparticles, with an infinity amount of quencher with an association constant, K_{app} [29,30,42]. We multiply both sides of Eq. (1) by I_0 to deliver the I_{surf}/I_0 from the intercept as indicated in Eq. (2). To elucidate the detailed effect of MeOH and TEOA on the electron injection at dye/oxide nanoparticle interfaces reflected as the fluorescence quenching and the capability of photocatalytic H_2 evolution, both of normal and reciprocal Stern–Volmer plots and the values calculated from the reciprocal Stern–Volmer plots are exhibited in Fig. 2 and Table 2, respectively. A correlation between low value of I_{surf}/I_0 and H_2 evolution for each TiO_2/TEOA and SnO_2/MeOH in Table 2 indicates that the sufficient electron injection from photo-excited dye-sensitizers to oxide nanoparticles is required for efficient H_2 evolution as higher values of I_{surf}/I_0 imply lower electron injection efficiency. Additionally the association constant of dye-sensitizers with oxide nanoparticles is typically observed to be lower in TEOA solution than that in MeOH solution, probably because of higher pH value in TEOA solution than that in MeOH solution due to the hydrolysis of the bonding between the Ti and carboxylate [29,30]. It is however indicated that the association constants are less likely to be related to the efficiency of H_2 evolution. Therefore the inverted results of H_2 evolution with TiO_2 and SnO_2 either in TEOA or MeOH are clearly attributed to the limiting factor of electron injection efficiency. This electron injection efficiency is the first factor determining the H_2 evolution in the system. And interestingly the injection efficiency is significantly affected by the combination of oxide semiconductor and sorrowing co-existing species either accepting or inhibiting the electron transfer at oxide/dye-sensitizer interface.

$$\frac{1}{I_0 - I} = \frac{1}{I_0 - I_{surf}} + \frac{1}{K_{app}(I_0 - I_{surf})[Q]} \tag{1}$$

$$\frac{I_0}{I_0 - I} = \frac{I}{I_0 - I_{surf}} + \frac{I_0}{K_{app}(I_0 - I_{surf})[Q]} \tag{2}$$

To elucidate the conjugated effect of MeOH addition in TEOA (0.3 M) and TEOA addition in MeOH (6.2 M) solutions on electron injection at dye/semiconductor interfaces reflected as the

Table 2
Photochemical properties calculated from the reciprocal Stern–Volmer plots in Fig.2.

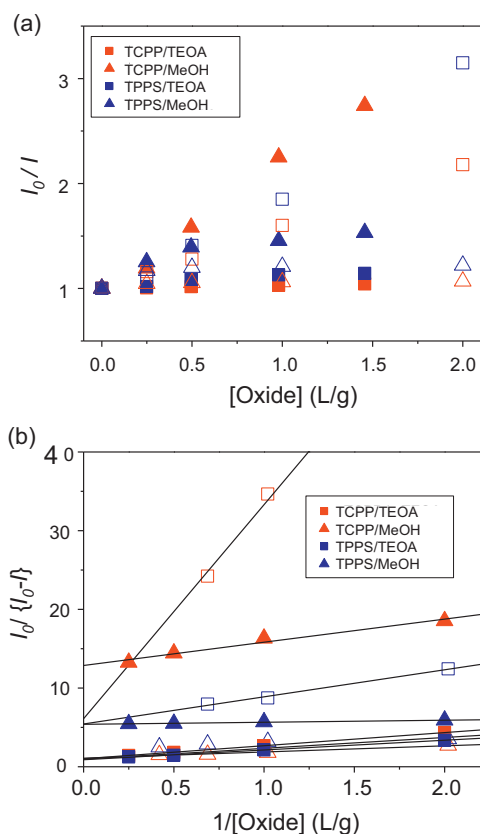|	TiO$_2$				SnO$_2$			
Dye-sensitizer	TCPP		TPPS		TCPP		TPPS	
Electron donor	TEOA	MeOH	TEOA	MeOH	TEOA	MeOH	TEOA	MeOH
$I_0/(I_0-I_{surf})$	1.02	12.9	0.892	5.4	6.10	1.09	5.43	0.96
$1-(I_{surf}/I_0)$	0.985	0.0776	1.12	0.185	0.164	0.917	0.184	1.046
(I_{surf}/I_0)	0.0149	0.922	−0.121	0.815	0.836	0.082	0.816	−0.05
$I_0/K_{app}(I_0-I_{surf})$	1.67	2.94	1.24	0.262	27.2	0.785	3.44	1.38
K_{app}	0.61	4.37	0.719	20.6	0.224	1.39	1.58	0.694
H$_2$ evolution (μmol)	9.2	0	8.4	0	Trace	6.6	Trace	5.1

Fig. 2. (a) Normal Stern–Volmer plot and (b) reciprocal Stern–Volmer plot of porphyrin dye-sensitized SnO$_2$ (filled plots) and TiO$_2$ (opened plots) with TCPP (red) and TPPS (blue) in the aqueous solution of co-existing electron donor, either MeOH (6.2 M) (triangle) or TEOA (0.3 M) (square). (For interpretation of the references to color in this figure legend, the reader is referred to the web version of this article.)

Fig. 3. H$_2$ evolution (opened plots) and the value of I_{surf}/I_0 (filled plots) calculated from the reciprocal Stern–Volmer plots of TCPP/TiO$_2$ (red) and TCPP/SnO$_2$ (blue) as a function of the concentrations of co-existing electron donor, (a) MeOH in TEOA (0.3 M) and (b) TEOA in MeOH (6.2 M), aqueous solutions. (For interpretation of the references to color in this figure legend, the reader is referred to the web version of this article.)

fluorescence quenching and the capability of photocatalytic H$_2$ evolution, I_{surf}/I_0 calculated from the reciprocal Stern–Volmer plots are overlaid on the H$_2$ evolution as a function of the concentrations of aqueous solutions of co-existing electron donor in TCPP dye-sensitized TiO$_2$ and SnO$_2$ nanoparticle suspension systems as shown in Fig. 3. Fig. 3a shows that the electron injection efficiency of TCPP/TiO$_2$ evaluated from the value of I_{surf}/I_0 remains stationary at low value in TEOA (0.3 M) system with MeOH addition. The MeOH addition in TEOA thus does not affect to the electron injection efficiency. This is because of the effect of TEOA as the promoter of electron injection with TCPP/TiO$_2$ system as we reported recently [29]. Fig. 3b also indicates that TEOA promotes the electron injection from photo-excited dye to TiO$_2$; *i.e.* TEOA significantly decreases the value of I_{surf}/I_0 by addition of TEOA ($\sim10^{-2}$ M) in MeOH, resulting in the enhancement in the electron injection.

On the other hand, pure MeOH solution roles as the suppressor of the electron injection from photo-excited dye-sensitizer to
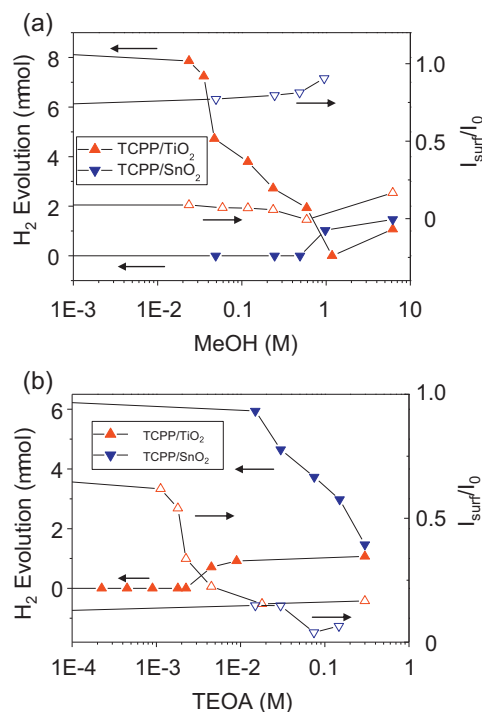
TiO$_2$ as discussed above (Table 1). We, however, reported another effect of MeOH, once MeOH was added in the co-existing electron promoter, TEOA. MeOH addition in TEOA solution with TCPP/TiO$_2$ induced another determinant factor of the H$_2$ evolution, that is, the recombination as the deactivation process of the electron in the semiconductor [30]. In fact, MeOH addition in TEOA solution did not reveal the suppression of the electron injection efficiency, while MeOH addition degraded the efficiency of H$_2$ evolution (Fig. 3a). We attributed this suppression of H$_2$ evolution in TEOA by addition of MeOH to the other dominant factor of recombination of electron with oxidized dye-sensitizers negatively affecting the efficiency of H$_2$ evolution, and which was also related to the conduction band shift of TiO$_2$ induced by MeOH addition [30]. We thus proposed that the H$_2$ evolution is dominated by two fundamental processes of electron transport, the injection and the recombination.

On contrary to the TCPP/TiO$_2$ system, TCPP/SnO$_2$ system revealed significant difference in these two electron transfer processes, injection and recombination, resulting in H$_2$ evolution (Fig. 3). As noticed in Table 1, TEOA and MeOH result in completely opposite effect on the H$_2$ evolution of TCPP/SnO$_2$ system

as compared with TCPP/TiO$_2$ system. Nevertheless, the electron transport process affected by co-existing species, TEOA and MeOH, revealed characteristic difference in TCPP/TiO$_2$ and TCPP/SnO$_2$ systems based on the reciprocal Stern–Volmer analysis. As TCPP/SnO$_2$ evolves no H$_2$ evolution in TEOA solution, this could be because of the low electron injection efficiency associated with modestly high value of I_{surf}/I_0, ~0.7 (Fig. 3a). The efficiency of H$_2$ was, however, improved by addition of more than 1 M of MeOH in TEOA solution, although the value of I_{surf}/I_0 is stationary at ~0.7 over the range of MeOH concentration in TEOA solution. Therefore the low ability of photocatalytic H$_2$ evolution could be associated with the two factors; low efficiency of the electron injection and rapid charge recombination with TEOA. Whereas, once the MeOH concentration reaches certain level, ~1 M, the charge recombination pass is possibly suppressed by the adsorbed MeOH and certain amount of H$_2$ is consequently evolved by TCPP/SnO$_2$ under irradiation (Fig. 3a).

On the other hand, TCPP/SnO$_2$ in MeOH solution results in high efficiency of H$_2$ evolution under irradiation. This is attributed to the efficient electron injection indicated by the low value of I_{surf}/I_0, with TCPP/SnO$_2$ in the corresponding MeOH solution (Fig. 3b). Whereas, the significant degradation of H$_2$ evolution was observed by addition of TEOA (>10^{-2} M) in MeOH solution. As the value of I_{surf}/I_0, remains sufficiently at low over the range of TEOA concentration, the results of H$_2$ evolution are not attributed to the suppression of the electron injection but the charge recombination process following the electron injection process. Therefore the photochemical analysis based on Stern–Volmer analysis revealed the significant differences in charge transfer kinetics of TCPP-sensitized TiO$_2$ and SnO$_2$ affected by the co-existing species, MeOH and TEOA, and therefore resulting in the difference of H$_2$ evolution under irradiation.

In addition to the electron injection efficiency, the association constants, K_{app}, of dye-sensitizers with oxide semiconductor nanoparticles were also calculated from the reciprocal Stern–Volmer plots and overlaid on the H$_2$ evolution as a function of the concentrations of co-existing electron donors, either MeOH added in TEOA (0.3 M) or TEOA added MeOH (6.2 M) aqueous solutions as shown in Fig. 4. This plot indicates similar trends between H$_2$ evolution and association constants, K_{app}, of dye-sensitizers with both TiO$_2$ and SnO$_2$ nanoparticles in case the electron injection efficiency is not the dominant factor of H$_2$ evolution, *i.e.* MeOH addition in TEOA with TCPP/TiO$_2$ system (Fig. 4a) and TEOA addition in MeOH with TCPP/SnO$_2$ system (Fig. 4b). In these cases, we also found that the threshold concentration of additional co-existing species revealing reduction of H$_2$ evolution is coincidentally matched at around 10^{-2} M for both MeOH addition in TEOA with TCPP/TiO$_2$ and TEOA addition in MeOH with TCPP/SnO$_2$ systems. These results clearly indicate that the recombination process is related to the dye-sensitizer adsorption/desorption nature on oxide semiconductors; *i.e.* the desorption of dye-sensitizer increases the recombination dominating the efficiency of H$_2$ evolution. However less correlation between H$_2$ evolution and association constants, K_{app}, of TCPP with both TiO$_2$ and SnO$_2$ nanoparticles was observed with TEOA addition in MeOH with TCPP/TiO$_2$ (Fig. 4b) and MeOH addition in TEOA with TCPP/SnO$_2$ (Fig. 4a) systems. This is probably because these two systems are presumably dominated by the injection efficiency, as discussed above. One can however notice that the higher association constant the system has the higher H$_2$ evolution is observed in Fig. 4, although the concentration range of additional co-existing species providing the transition of association constant is not always correlated to the H$_2$ evolution. This relation presumably supports that the injection process and recombination process are strongly influenced by the adsorption nature of dye-sensitizers affecting the molecular orbital of dye-sensitizer coupling to the density of state of the oxide semiconductor as the determinants
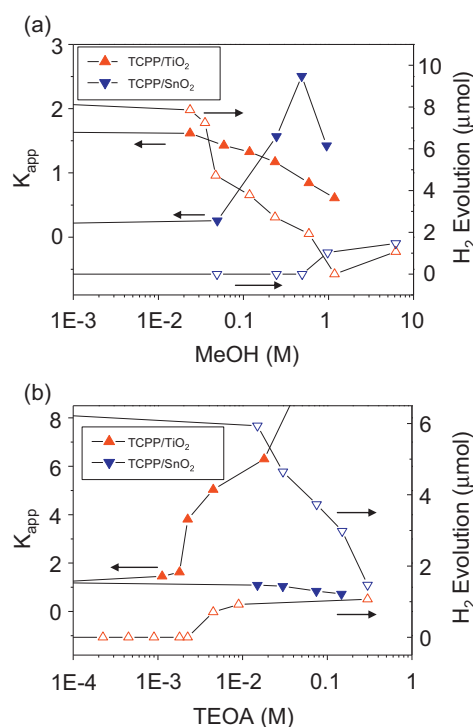

Fig. 4. The association constants (filled plots) calculated from the reciprocal Stern–Volmer plots and H$_2$ evolution (opened plots) of TCPP/TiO$_2$ (red) and TCPP/SnO$_2$ (blue) as a function of the concentrations of co-existing electron donor, (a) MeOH in TEOA (0.3 M) and (b) TEOA in MeOH (6.2 M), aqueous solutions. (For interpretation of the references to color in this figure legend, the reader is referred to the web version of this article.)

of the interfacial electron transfer process, injection and recombination [17–21]. Therefore the overall H$_2$ evolution as the result of the whole competitive electron transfer processes in dye-sensitized semiconductor is strongly influenced by the environment affecting the adsorption nature of dye-sensitizers on the semiconductors. The discrepancy of the results of association constants varied with addition of co-existing species and the results of H2 evolution observed in Fig. 4 is therefore attributed to the complicated effect of dye-adsorption nature to both injection and recombination, probably in addition to many factors, such as the trap density of oxides, interfacial dipole moment of sensitizers, the conduction band shift, adsorption of co-existing species, and protonation of oxide surface.

3.3. Photoelectrochemical analysis of dye-sensitized nanoporous oxide films

Since the Ru sensitizer, N719, not possessing enough intensity of fluorescence cannot be applied to Stern–Volmer analysis, the photoelectrochemical analyses were carried out with N719 dye-sensitized TiO$_2$ and SnO$_2$ porous films in aqueous solution of electron donors, MeOH and TEOA, under visible light irradiation (>410 nm Xe lamp). The photocurrent and dark current responded to a manipulated shutter with working electrode potential of 0.1 V (*vs.* Ag/AgCl) as shown in Fig. 5. Since the Fermi level of the oxide semiconductor working electrode was controlled at the certain potential locating within the band gap of oxide and more negative than oxidation potential of dye-sensitizer, dark current does not appear and the photocurrent is efficiently extracted. Therefore the photocurrent is determined mainly by the electron injection from dye-sensitizer to oxide semiconductor [5,6]. The photocurrent in Fig. 5 exhibited a stable current with N719/TiO$_2$ both in TEOA (0.3 M) and MeOH (6.2 M) aqueous solutions, and therefore the results are consistent with the H$_2$ evolution in
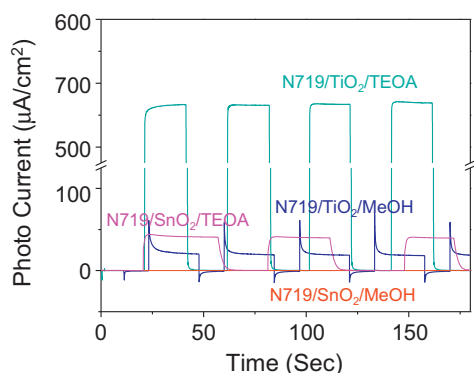
Fig. 5. Photocurrent-dark current response of N719/TiO$_2$ or N719/SnO$_2$ porous films either in TEOA (0.3 M) or MeOH (6.2 M) aqueous solutions revealing constant photocurrent at a potential of 0.1 V vs. Ag/AgCl.

Table 1. On the other hand, N719/SnO$_2$ revealed different feature; thus the photocurrent was observed with dye-sensitized SnO$_2$ film in TEOA solution, while not in MeOH solution under irradiation. Although N719/SnO$_2$ in both of TEOA and MeOH solution revealed no H$_2$ evolution, these results clearly indicate that the photocatalytic activity of H$_2$ evolution is attributed to not only the electron injection from dye-sensitizer but also the following electron transfer process, recombination process. According to these photo-electrochemical results, no H$_2$ evolution with N719/SnO$_2$ in MeOH solution is attributed to little injection efficiency, while no H$_2$ evolution with N719/SnO$_2$ in TEOA is attributed to the recombination probably promoted by TEOA, since the observed photocurrent with N719/SnO$_2$ in TEOA was substantially higher than that with N719/TiO$_2$ in MeOH. This result with N719/SnO$_2$ is completely opposite to the results with

TCPP/SnO$_2$ with the results indicating little injection in TEOA and substantial injection in MeOH solution (Table 1). We therefore observed that the effect of co-existing species varies not only with the combination between the donor species and oxide semiconductor, but also the donor species and dye-sensitizer, although the interfacial characteristics are supposed to be similar due to same carboxylic acid linker of dye-sensitizer on oxide semiconductor. Furthermore, the discrepancy between the amplitude of the photocurrent in dye-sensitized porous oxide films and the H$_2$ evolution was also observed probably due to the balance of electron injection and charge recombination; e.g. N719/TiO$_2$ in MeOH providing much lower photocurrent than that in TEOA with the factor of ~10 results in comparable H$_2$ evolution in both MeOH and TEOA solutions.

To elucidate further insight of the electronic characteristics of N719-sensitized oxide semiconductors, the cyclic voltammograms of N719/TiO$_2$ and N719/SnO$_2$ porous films either in TEOA (0.3 M) or MeOH (6.2 M) aqueous solutions were obtained as shown in Fig. 6. Clear difference was observed as the onset potential of cathodic current in each system quantitatively indicating the structure of density state of the electron at conduction band edges of each semiconductor porous film. N719/TiO$_2$ revealed the flat curve in the middle potential region and cathodic current with the onset potential in the negative potential region. These are attributed to the no current flow at the potential region of band gap and the trap filling cathodic current at near conduction band edge, respectively [43]. Since the conduction band of TiO$_2$ is shifted following the Nernstian behavior correlated to pH values in the surrounding solution with the magnitude of 59 meV/pH unit [44], the large difference of the onset potentials of cathodic current with N719/TiO$_2$ in MeOH and TEOA (Fig. 6a and b) is attributed to the potential shift of the conduction band due to the pH difference in the surrounding solution (S4). According to the Nernstian behavior of the
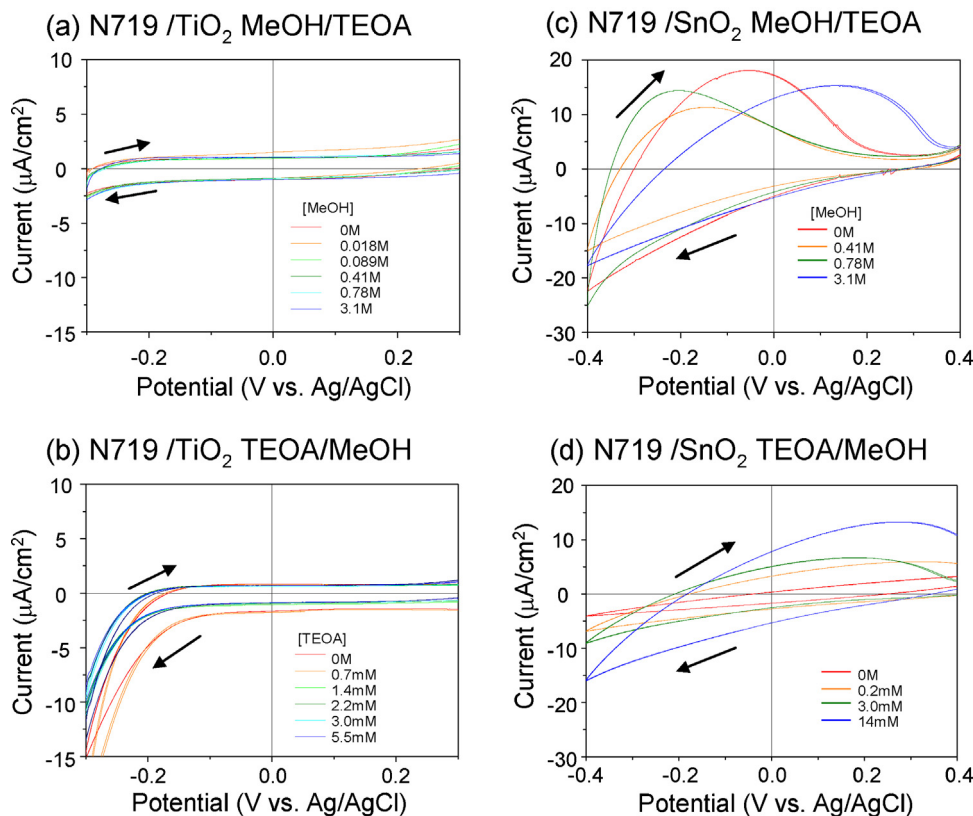

Fig. 6. Cyclic voltammograms of N719/TiO$_2$ (a and b) and N719/SnO$_2$ (c and d) porous films either in TEOA (0.3 M) (a and c) or MeOH (6.2 M) (b and d) aqueous solutions with addition of another electron donors as corresponding to Fig. 5.

conduction band, the pH change by addition of MeOH or TEOA, pH 6–11, is consistent to the difference of onset potential, ∼250 mV, in MeOH and TEOA (Fig. 6a and b). As the cyclic potential sweep does not exhibit any of anodic current typically representing the extraction of trapped electron in the TiO_2 film, the proton reduction occurs by the electron at the surface of TiO_2 possessing small density of state as the trap state in the inter-band of TiO_2. On the other hand, $N719/SnO_2$ revealed the relatively large cathodic current with more positive onset potential of cathodic current attributed to the density state in the inter-band region probably due to relatively more trap state in SnO_2 than TiO_2 (Fig. 6c and d). Even the reverse potential cycle exhibits the reversible anodic current corresponding to the discharging processes of trap state in SnO_2 porous films (Fig. 6c and d). This indicates that $N719/SnO_2$ does not have the enough ability to reduce protons in the solution. This is probably related to the more trap states in the inter-band region of SnO_2 resulting in the lower potential level of electron in the trap state of SnO_2. As the result, the large density of trap state on SnO_2 observed in Fig. 6c and d could lowers the potential of the injected electron, quasi-Felmi level, to become unable to reduce proton in the aqueous solution even in case the dye-sensitizer injects the electrons to SnO_2 under irradiation, though the dye-sensitizers are able to inject sufficient electrons in $N719/SnO_2$ in TEOA solution indicated in Fig. 5. Although $N719/SnO_2$ in MeOH solution revealed relatively less trap state than that in TEOA solution (Fig. 6d), $N719/SnO_2$ in MeOH does not inject electron into SnO_2 as indicated in the photoelectrochemical analysis (Fig. 5). As the result, neither of $N719/SnO_2$ in MeOH nor TEOA exhibited H_2 evolution, while each mechanism is different as observed with porphyline sensitizer.

As we have already reported, the electron injection and charge recombination are determinant factors of dye-sensitized oxide nanoparticles [29,30]. Although similar results were observed in dye-sensitized TiO_2 and SnO_2, H_2 evolution revealed completely opposite results at a glance. It was, however, clearly elucidated by photochemical and photoelectrochemical analysis that the H_2 evolution was resulted from not commonly applied simple mechanism of electron injection from dye due to the difference of conduction band energy level relative to the LUMO of dye-sensitizer but convolution of both electron injection and charge recombination kinetics significantly influenced by the co-existing species, MeOH and TEOA, in the surrounding medium. Therefore these differences between TiO_2 and SnO_2 cannot be explained based on only the conduction band potential difference of TiO_2 and SnO_2, but also more complicated mechanisms, *e.g.* involving adsorption/desorption dynamics of co-existing species and dye-sensitizers and trap states mostly induced by the surface state of semiconductors, possibly influencing to the electron transfer processes, such as electron injection and charge recombination at the interfaces [23,45].

4. Conclusion

We applied dye-sensitized nanocrystalline TiO_2, SnO_2, and ZnO colloidal suspension in aqueous system for H_2 evolution under visible light (>390 nm). The efficiency of H_2 evolution was strongly influenced by the oxide semiconductor, TiO_2, SnO_2, and ZnO, with dye-sensitizers, N719 and porphyline derivatives, TCPP and TPPS, in addition to the co-existing electron donor species, MeOH and TEOA, in the colloidal suspension system. The analysis of the fluorescence quenching of dye-sensitizer in colloidal suspensions based on the reciprocal Stern–Volmer relation and the photoelectrochemical analysis of dye-sensitized oxide nanoporous films revealed the major variation of electron injection and following process of charge recombination kinetics with the combination of the oxide semiconductors, dye-sensitizers, and electron donor aqueous solutions. The correlation between the H_2 evolution and the

association constants of dye-sensitizers on oxide semiconductors could attributes the efficiency of H_2 evolution to the primary electron injection process and following recombination kinetics significantly influenced by the adsorption–desorption nature of dye-sensitizers and co-existing electron donor species, MeOH and TEOA. The observed results of H_2 evolution by varying dye-sensitizers, semiconductors, and co-existing electron donor species is clearly originated by the surface chemical nature of semiconductors with dye-sensitizers and co-existing species rather than simple conduction band energy level of semiconductor which typically utilized to discuss the results of H_2 evolution. Therefore the proper combination of co-existing electron donor species with certain dye-sensitizer results in significant improvement of the conversion efficiency of H_2 evolutions under visible light. We also revealed that this is not originated to the conduction band shift of oxide semiconductors by changing the pH value of surrounding solution which is typically discussed. More interestingly the co-existing species, MeOH and TEOA, revealed the opposite effect for TiO_2 and SnO_2 in terms of H_2 evolution, while we revealed that the opposite results are attributed to the completely different electron transport mechanism. Although further detail has to be studied, the combinational effect among oxide semiconductors, dye-sensitizers, and co-existing species in surrounding medium is quite important for not only the photocatalysts but also the photovoltaics using dye-sensitization of oxide nanoparticles in order to achieve higher conversion efficiency.

Appendix A. Supplementary data

Supplementary data associated with this article can be found, in the online version, at http://dx.doi.org/10.1016/j.apcatb.2013.10.016.

References

[1] X. Chen, S. Shen, L. Guo, S.S. Mao, Chem. Rev. 110 (2010) 6503–6570.
[2] A. Fujishima, X. Zhang, D.A. Tryk, Surf. Sci. Rep. 63 (2008) 515–582.
[3] M.G. Walter, E.L. Warren, J.R. McKone, S.W. Boettcher, Q. Mi, E.A. Santori, N.W. Lewis, Chem. Rev. 110 (2010) 6446–6473.
[4] A. Hagfeldt, M. Grätzel, Chem. Rev. 95 (1995) 49–68.
[5] B. O'Regan, M. Grätzel, Nature 353 (1991) 737–740.
[6] A. Hagfeldt, G. Boschloo, L. Sun, L. Kloo, H. Pettersson, Chem. Rev. 110 (2010) 6595–6663.
[7] R. Abe, K. Hara, K. Sayama, K. Domen, H. Arakawa, J. Photochem. Photobiol. A 137 (2000) 63–69.
[8] Z. Jin, X. Zhang, G. Lu, S. Li, J. Mol. Catal. A 259 (2006) 275–280.
[9] W.J. Youngblood, S.-H.A. Lee, Y. Kobayashi, E.A. Hernandez-Pagan, P.G. Hoertz, T.A. Moore, A.L. Moore, D. Gust, T.E. Mallouk, J. Am. Chem. Soc. 131 (2009) 926–927.
[10] A. Harriman, I.J. Pickering, J.M. Thomas, P.A. Christensen, J. Chem Soc, Faraday Trans. I 84 (1988) 2795–2806.
[11] R.H. Nakamura, Frei, J. Am. Chem. Soc. 128 (2006) 10668–10669.
[12] B.C. O'Regan, J.R. Durrant, Acc. Chem. Res. 42 (2009) 1799–1808.
[13] K. Hara, T. Sato, R. Katoh, A. Furube, Y. Ohga, A. Shinpo, S. Suga, K. Sayama, H. Sugihara, H. Arakawa, J. Phys. Chem. B 107 (2003) 597–606.
[14] Y. Tachibana, M.K. Nazeeruddin, M. Grätzel, D.R. Klug, J.R. Durrant, Chem. Phys. 285 (2002) 127–132.
[15] K. Kalyanasundaram, N. Vlachopoulos, V. Krishnan, A. Monnier, M. Grätzel, J. Phys. Chem. 91 (1987) 2342–2347.
[16] J.B. Asbury, N.A. Anderson, E. Hao, X. Ai, T. Lian, J. Phys. Chem. B 107 (2003) 7376–7386.
[17] J.-H. Yum, S.-R. Jang, R. Humphry-Baker, M. Grätzel, J.-J. Cid, T. Torres, M.K. Nazeeruddin, Langmuir 24 (2008) 5636–5640.
[18] A. Kay, M. Grätzel, J. Phys. Chem. 97 (1993) 6272–6277.
[19] N.R. Neale, N. Kopidakis, J. van de Lagemaat, M. Grätzel, A.J. Frank, J. Phys. Chem. B 109 (2005) 23183–23189.
[20] D.F. Watson, G.J. Meyer, Coord. Chem. Rev. 248 (2004) 1391–1406.
[21] J.A. Pollard, D.S. Zhang, J.A. Downing, F.J. Knorr, J.L. McHale, J. Phys. Chem. A 109 (2005) 11443–11452.
[22] D.N. Furlong, D. Wells, W.H.F. Sasse, J. Phys. Chem. 90 (1986) 1107–1115.
[23] K. Gurunathan, P. Maruthamuthu, V.C. Sastri, Int. J. Hydrogen Energy 22 (1997) 57–62.
[24] S.K. Choi, H.S. Yang, J.H. Kim, H. Park, Appl. Catal., B 121–122 (2012) 206–213.
[25] K. Kalyanasundaram, J. Kiwi, M. Grätzel, Helv. Chim. Acta 61 (1978) 2720–2730.

[26] M.D. Hernández-Alonso, F. Fresno, S. Suárez, J.M. Coronado, Energy Environ. Sci. 2 (2009) 1231–1257.
[27] L. Zhang, W. Wang, S. Sun, Y. Sun, E. Gao, J. Xu, Appl. Catal., B 132–133 (2013) 315–320.
[28] C. Zhan, M.M. Maitani, D. Mochizuki, E. Suzuki, Y. Wada, Chem. Lett. 41 (4) (2012) 423–424.
[29] M.M. Maitani, C. Zhan, C.-C. Huang, C.-C. Hu, D. Mochizuki, E. Suzuki, Y. Wada, Bull. Chem. Soc. Japan 85 (2012) 1268–1276.
[30] M.M. Maitani, C. Zhan, D. Mochizuki, E. Suzuki, Y. Wada, Appl. Catal., B 140–141 (2013) 406–411.
[31] S. Li, G. Ni, L. Bo, M. Chen, W. Yang, J. Gao, X. Li, X. Guo, Q. Xue, Synth. React. Inorg. Met.-Organ. Nano-Met. Chem. 35 (2005) 669–676.
[32] C.J. Barbe, F. Arendse, P. Comte, M. Jirousek, F. Lenzmann, V. Shklover, M. Grätzel, J. Am. Ceram. Soc. 80 (1997) 3157–3171.
[33] T. Iwasita, Electrochim. Acta 47 (2002) 3663–3674.
[34] S. Wasmus, A. Küver, J. Electroanal. Chem. 461 (1999) 14–31.
[35] M. Kirch, J.-M. Lehn, J.-P. Sauvage, Helv. Chim. Acta 62 (1979) 1345–1384.
[36] K. Kalyanasundaram, M. Neumann-Spallart, J. Phys. Chem. 86 (1982) 5163–5169.
[37] A. Kathiravan, R. Renganathan, J. Colloid Interface Sci. 331 (2009) 401–407.
[38] M.K. Nazeeruddin, A. Kay, I. Rodicio, R. Humphry-Baker, E. Miiller, P. Liska, N. Vlachopoulos, M. Grätzel, J. Am. Chem. Soc. 115 (1993) 6382–6390.
[39] S. Hirayama, J. Chem. Soc., Faraday Trans. I 78 (1982) 2411–2421.
[40] J.M. Masnovi, E.D. Seddon, J.K. Kochi, Can. J. Chem. 62 (1984) 2552–2559.
[41] P.V. Kamat, W.E. Ford, Chem. Phys. Lett. 135 (1987) 421–426.
[42] P.V. Kamat, J.-P. Chauvet, R.W. Fessenden, J. Phys. Chem. 90 (1986) 1389–1394.
[43] G. Boschloo, D. Fitzmaurice, J. Phys. Chem. B 103 (1999) 2228–2231.
[44] (a) T. Watanabe, A. Fujishima, K.-I. Honda, Chem. Lett. (1974) 897–900;
(b) J.M. Bolts, M.S. Wrighton, J. Phys. Chem. 80 (1976) 2641–2645.
[45] (a) C.X. She, J.C. Guo, T.Q. Lian, J. Phys. Chem. B 111 (2007) 6903–6912.